International Journal of Applied Earth Observations and Geoinformation 95 (2021) 102251

Contents lists available at ScienceDirect

International Journal of Applied Earth Observations and Geoinformation

journal homepage: www.elsevier.com/locate/jag

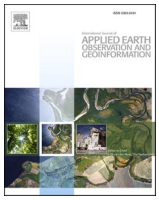

Monitoring temporal variations in the geothermal activity of Miocene Lesvos volcanic field using remote sensing techniques and MODIS – LST imagery

Sophia Peleli [a], Maria Kouli [a,b,c,*], Francesco Marchese [d], Teodosio Lacava [d], Filippos Vallianatos [a,b,e], Valerio Tramutoli [f]

[a] Hellenic Mediterranean University, UNESCO Chair on Solid Earth Physics & Geohazards Risk Reduction, Chania, Crete, Greece
[b] Hellenic Mediterranean University, Institute of Physics of the Earth's Interior & Geohazards, Chania, Crete, Greece
[c] Hellenic Mediterranean University, Faculty of Electronic Engineering, Chania, Crete, Greece
[d] National Research Council, Institute of Methodologies for Environmental Analysis, Tito Scalo (PZ), Italy
[e] National and Kapodistrian University of Athens, Faculty of Geology and Geoenvironment, Athens, Greece
[f] University of Basilicata, School of Engineering, Potenza, Italy

ARTICLE INFO

Keywords:
Lesvos volcanic field
Land Surface Temperature – LST
MODIS
RETIRA-index
Geothermal anomalies

ABSTRACT

Many islands of the Aegean Sea show strong geothermal activity due to volcanism in the area. In this paper, Robust Satellite Techniques (RST) are used to isolate, from other known possible sources, those thermal anomalies possibly related to geothermal activity in the Miocene volcanic field of Lesvos Island (Northern Aegean). For this purpose, 12 years (2003–2014) of daily Night-time Land Surface Temperature (LST) products, from Moderate Resolution Imaging Spectroradiometer (MODIS) acquisitions were analyzed. The final dataset contained 770 thermal anomalies whose spatial correlation with geological and structural data of Lesvos - such as caldera rims, ring faults, major tectonic lineaments and hydrothermal alterations mapped by processing SENTINEL-2 MSI satellite images – has been particularly investigated. In the approximately 20 ma geothermal field of Lesvos, geothermal activity seems to be also associated with the extensional regime of the broader area that leads to lithosphere thinning and consequent heat transfer in the multi-fractured terrain of Lesvos through volcanic and tectonic faults. Achieved results seem to confirm the possibility to use RST-based thermal anomalies to identify temporal variations in the geothermal activity probably due to the uplifting and circulation of the hydrothermal waters.

1. Introduction

Geothermal fields are those where an increased heat flow creates positive (spatial) temperature anomalies. A geothermal field is typically connected with volcanic activity and related structures and phenomena such as calderas, lava domes, pyroclastic rocks, thermal (hot) springs, overall circulation of thermal waters, hydrothermal alterations and mineralization. Moreover, the faults in active extensional tectonic environments also play an important role in the deep circulation of geothermal fluids as well as in heat transfer from deep to shallow crustal levels (Faulds et al., 2006; Faulds and Henry, 2008; Hacioglou et al., 2020; Moeck, 2014). Such tectonic environments are subject to lithosphere thinning and crustal extension and are related to structurally controlled heat transport and fluid flow. In such seismically active areas, temporal variations in the geothermal system characteristics (i.e. geochemistry, temperature) can reflect changes in the sub-surface physicochemical processes, such as fluid mixing, micro-fracturing, permeability changes (Li et al., 2013; Littlefield and Calvin, 2014) and episodic gas injection into the hydrothermal system (Cannatelli et al., 2020). According to Faulds et al. (2012), without recent magmatism, extensional or transtensional deformation is a non-negotiable component in generating viable geothermal systems. Spatially, geothermal fields are usually controlled by the existence of high permeability structures which act as pathways to fluid circulation. These structures can be both ring and radial faults which are connected with the evolution of calderas and/or tectonic lineaments. As a result, a close spatial

* Corresponding author at: Hellenic Mediterranean University, Institute of Physics of the Earth's Interior & Geohazards, Chania, Crete, Greece.
E-mail addresses: mkouli@hmu.gr (M. Kouli), francesco.marchese@imaa.cnr.it (F. Marchese), teodosio.lacava@imaa.cnr.it (T. Lacava), fvallian@yahoo.gr (F. Vallianatos), valerio.tramutoli@unibas.it (V. Tramutoli).

https://doi.org/10.1016/j.jag.2020.102251
Received 30 October 2019; Received in revised form 1 October 2020; Accepted 1 October 2020
Available online 29 October 2020

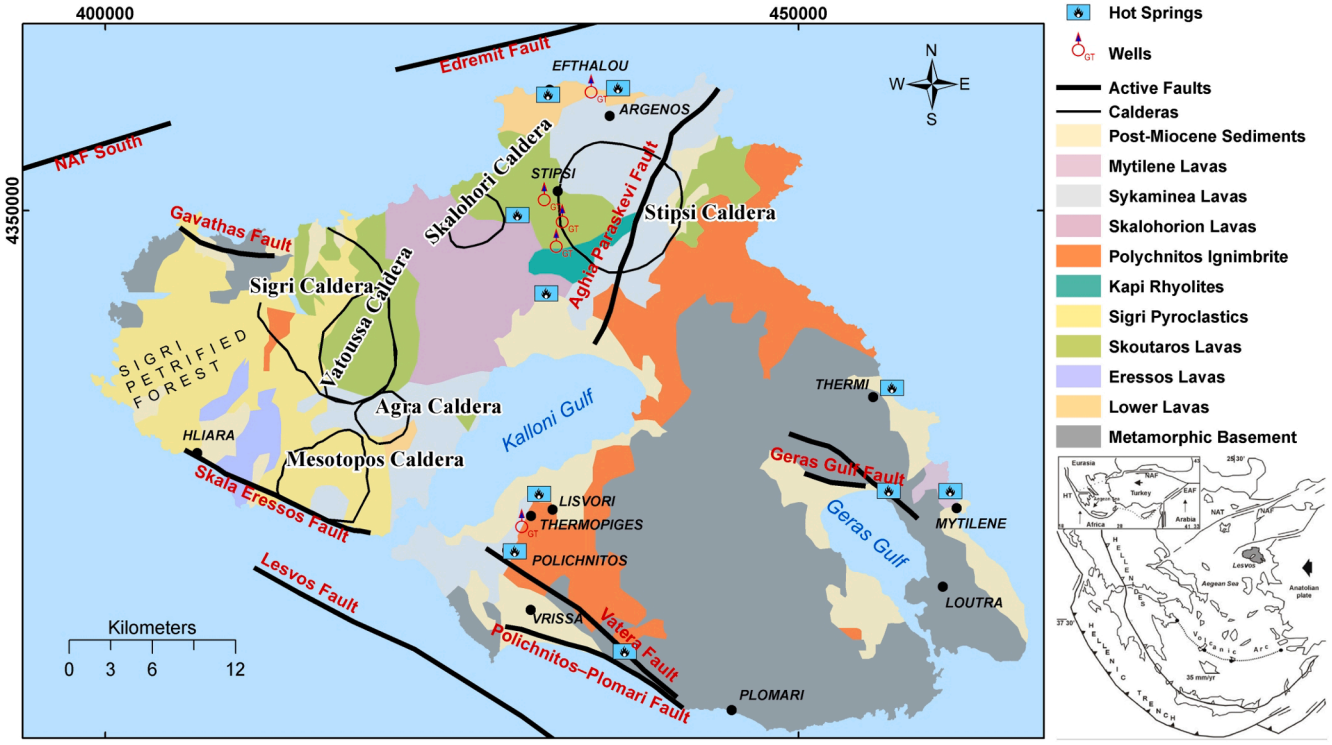

Fig. 1. Location map of Lesvos island with overlay of the caldera structures (adopted from Kouli and St. Seymour, 2006), hot springs and wells locations (after Mendrinos et al., 2010) and major active faults (adopted from Ganas et al., 2013). Inset: Map presenting the general geodynamic context in the eastern Mediterranean Sea. NAF: Northern Anatolian Fault, NAT: Northern Aegean Trough (modified from McKenzie, 1972).

relation between geothermal springs, hydrothermally altered rocks and epithermal mineralization with the aforementioned structures is usually reported (Krupp and Seward, 1987; Sillitoe, 1993; Rokos et al., 2000; Vamvoukakis et al., 2005; Guido and Campbell, 2011). In this direction, geothermal anomalies mapping is important for localization of mineral alterations and hydrothermal routes mapping.

Satellite sensors, such as MODIS (Moderate Resolution Imaging Spectroradiometer), having channels in the infrared bands, enable the monitoring of the Earth's thermal field at a 1 km spatial resolution (Lillesand et al., 1987; Anderson et al., 2012; Vollmer and Möllmann, 2017). Land Surface Temperature (LST) measures the emission thermal radiance from the land surface where the incoming solar energy interacts with objects and materials of different physicochemical properties. As a result, LST can greatly contribute to the understanding of of land surface processes in various scales (from local to global) (Brunsell and Gillies, 2003; Anderson and Kustas, 2008; Kustas and Anderson, 2009; Karnieli et al., 2010; Keramitsoglou et al., 2011; Christman et al., 2016; Scambos et al., 2018; Eleftheriou et al., 2018; Aguilar-Lome et al., 2019). Satellite remote sensing enables the estimation of LST over wide areas and especially in sites with different land surface characteristics, such as vegetation cover, topography, lithology, tectonic structure and geomorphometry with a variable spatio-temporal resolution depending on the selected satellite/sensor system (Li et al., 2013). Regional geothermal and structural characteristics such as volcanic fields, geothermal fields and geothermal springs that are also related to lithological, tectonic and hydrogeological features can also contribute to variability in the LST, in specific geological regimes (Zouzias et al., 2011). As a consequence, numerous satellite data have been incorporated for geothermal exploration and several studies have been carried out for monitoring geothermal fields by using the LST product (Lee, 1978; Prakash et al., 1995; Fred et al., 2008; Qin et al., 2011; Stroppiana et al., 2014). Regional geothermal fields have been successfully localized in the Aegean region by Zouzias et al. (2011) using LST terrain segmentation of temporal night-time MODIS-LST imagery. In another study, multi-temporal LST imagery contributed to the identification of a major geothermal field in the Afar Depression (Ethiopia), (Miliaresis, 2012). Moreover, two probable geothermal fields located under the zone of Tangshan in China, were detected using thermal infrared and LST maps (Li et al., 2012).

The RST (Robust Satellite Techniques; Tramutoli et al., 2005, 2007) technique is a known multi-temporal scheme of satellite data analysis devoted to highlights temporal anomalies in satellite imagery time-series. RST offers several advantages compared to other methods including the reduction of the "natural" (e.g. due to changes in atmospheric conditions, the spatio-temporal difference in land-covers, topography and weather conditions) and "observational" (e.g. incorrect image-to-image co-location, changes in view angles or in the hours of images collections) "noise".

Greece has inherited numerous thermal and mineral springs (Lambrakis et al., 2014) as a result of the volcanic and tectonic activity affecting the Hellenic area since Tertiary (Fytikas et al., 2005). In this work, we investigated the possibility to use the RST technique to identify possible temporal variations of the geothermal activity in the Lesvos Miocene (Greece) volcanic area (Fig. 1). To this aim, the RETIRA (Robust Estimator of TIR Anomalies; Tramutoli et al., 2001) index - an improved version of the generic ALICE (Absolutely *Llocal* Index of Change of Environment, Tramutoli, 1998) index – suitable for further reducing the effects of variable local meteo/climatic conditions, was computed over a dataset spanning over 12 years of MODIS satellite imagery.

2. The Lesvos miocene volcanic field

Lesvos Island is the third biggest Greek island and it is located in the Northern Aegean Sea region (Fig. 1). The shape of the island is formed by the gulfs of Kalloni in the southern coast and of Gera in the southeast (Fig. 1). The broad area is mainly characterized by a NE–SW and NW–SE oriented basin and range topography as a result of the Earth's crust

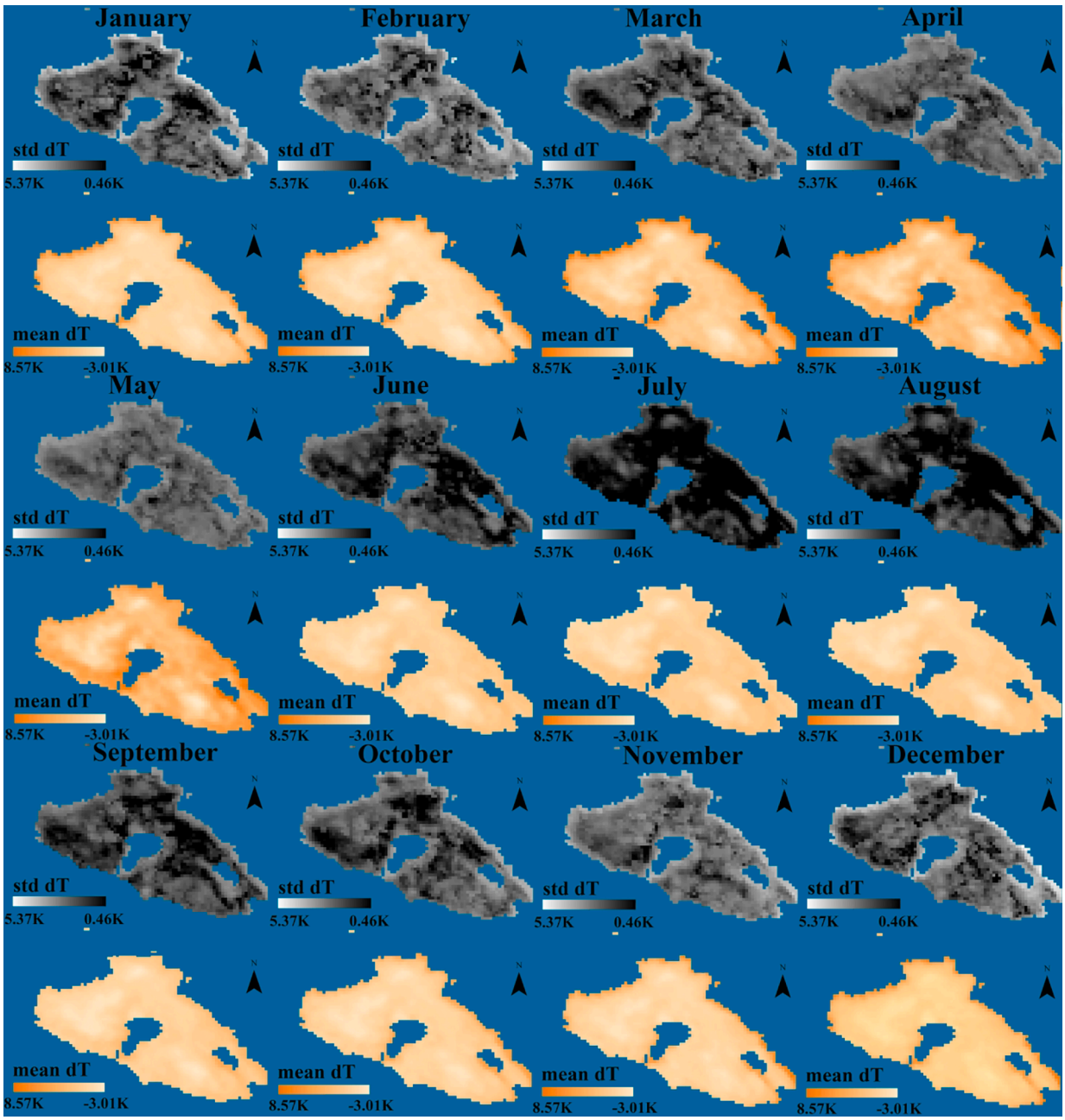

Fig. 2. Monthly reference fields $\mu_{\Delta T}(x,y)$ and $\sigma_{\Delta T}(x,y)$ calculated for all the months of the year on the basis of MODIS LST observations acquired over Lesvos island from January 2003 to December 2014. Color scale and contrast stretch is the same on all images.

extension and thinning since the Upper Miocene (Mercier et al., 1989; Roussos and Lyssimachou, 1991). The faulting in the area is controlled by the North Anatolian Fault (NAF) which westward is divided into two main branches (Jackson and McKenzie, 1988; Le Pichon et al., 1995; Le Pichon and Kreemer, 2010; Chatzipetros et al., 2013). Lesvos is located very close to the southernmost branch of the NAF, a major active deformation zone known as the Edremit fault (Fig. 1). Six major active normal and strike-slip tectonic faults/systems are located in the island (Fig. 1) (Chatzipetros et al., 2013; Ganas et al., 2013) and some of them are associated with thermal activity as is the case with the 13.5 long fault line in the areas of Polichnitos and Vatera fault system which seems to control the Polichnitos geothermal field (Günther et al., 1977) and the local thermal springs. Volcanic successions cover almost 70% of the island forming part of a belt of calc-alkaline and shoshonitic volcanic rocks in the northeastern Aegean and western Anatolia (Pe-Piper and Piper, 1993) (Fig. 1). The shoshonites are both underlain and overlain by calcalkaline volcanic rocks, and range in composition from andesite to rhyolite in the form of flows, domes and pyroclastic rocks (Pe-Piper and Piper, 1993). In the past, remote sensing techniques successfully identified six caldera structures (Kouli and St.Seymour, 2006) in the Lesvos heavily eroded Miocene volcanic field. Four of them (Sigri, Mesotopos, Agra and Skalohorion calderas) were identified for the first time using satellite image interpretation with the Stipsi and Vatoussa calderas being geometrically and spatially revised. To the north, a major caldera structure, the Stipsi caldera prevails. It is intersected by a major fault structure and exhibits extended hydrothermal alterations closely associated with epithermal gold systems along the ring and other faults. The intense hydrothermal alteration system extends to the south of Stipsi village, in the Kapi lava domes and in the external northern part of the caldera (Vamvoukakis et al., 2005). In the northwestern Lesvos, the

nested Sigri caldera is proposed to be the source of the renown Sigri Petrified Forest (Fig. 1) (Kouli and St.Seymour, 2006). This is one of the two largest Petrified Forests in the world, covering an area of 150 km^2 representing a World Heritage of UNESCO. The Sigri caldera encompasses the Vatoussa caldera, previously reported by Pe-Piper (1980). Its floor is characterized by a ring and rectilinear faults. Extensively hydrothermally altered lava domes are met in the southeastern part of the caldera (Vamvoukakis et al., 2005). The smaller Mesotopos caldera is located to the southwestern Lesvos. Radial and ring faults govern its drainage system. Lava domes are intruded through the radial faults and they are intensively altered. Agra and Skalohorion calderas are of small dimensions and not yet associated with known hydrothermal alterations (Vamvoukakis et al., 2005). These volcanic structures are potential hosts of epithermal gold mineralization due to the intensive hydrothermal activity that is extensively observed (Kelepertsis and Esson, 1987; Kelepertzis, 1993; Rokos et al., 2000; Vamvoukakis et al., 2005) and suitable targets for deep geothermal exploration (Mendrinos et al., 2010).

Mostly medium but also some high enthalpy geothermal fields associated with geothermal springs occur in Lesvos as a result of the volcanic activity that took place mainly during Miocene and the active extensional geodynamic context which is probably the reason why the geothermal field of Lesvos is still active despite its age. Specifically, many geothermal springs (50–85 °C) are located near the seashore in the northern and southeastern parts of Lesvos and inland of the Gulf of Kalloni (Fig. 1). The most important hot springs are in Polichnitos (one of the hottest in Europe), Lisvori, Thermi, Geras Bay, Eftalou, Argenos and near Plomari. In the hot springs of Polichnitos, the water temperature reaches 87.6 °C. Geothermal exploration of the island began in the late 1960s; Public Power Corporation (PPC) has opened production wells in the villages of Argenos and Stipsi at depths from 300 to 1085 m while one more production well 150 deep, was drilled in 2008 in the Polichnitos area providing geothermal waters of about 88 °C (Andritsos et al., 2010). According to Mendrinos et al. (2010), geothermal use on Lesvos involves thermal spas and heating of greenhouses, while exploration for deeper geothermal resources requiring drilling of a few kilometers deep wells.

3. Data

In this work, we used the MODIS Land Surface Temperature and Emissivity Daily L3 Global 1 km (MOD11_A1) product from Terra MODIS (i.e. the version 005 (V5)) available from March 5, 2000. The MOD11_A1 represents a gridded version of MOD11_L2 product with pixels that are projected to Earth locations on a sinusoidal mapping grid (Wan, 2006). This product has a spatial resolution of 1 km and guarantees an accuracy of 1 K under clear-sky conditions (e.g. Wan, 2006). The retrieved LST is not mixed with cloud-top temperature, while cloudy pixels are skipped using the MODIS cloud mask product (MOD35_L2 from Terra MODIS or MYD35_L2 from Aqua MODIS) (Wan, 2006). Night-time LST images were preferred are less affected by soil–air temperature differences than daytime data and less sensitive to local variations (due for instance to cloud cover or shadows) of solar illumination which could be one more source of variability of Land Surface Temperature. We analyzed 12 years of satellite records to compute the RETIRA index defined in Eq. (2). In detail, during the pre-processing phase, we isolated the "Night-time Land Surface Temperature" layer dataset and all the images were spatially clipped over the Lesvos Island area. Monthly reference fields $\mu_{\Delta T}(x,y)$ and $\sigma_{\Delta T}(x,y)$ were then generated for all the months of the year observations acquired over Lesvos island from January 2003 to December 2014 (Fig. 2). In some case, the measurements of TIR anomalies can exhibit particularly high values due to natural (e.g. extremely warm days, floods or precedent rains which increase soil emissivity), wildfires, cloud coverage (and related greenhouse effects) and/or observational (e.g. inaccurate image navigation/co-location) conditions. Due to its statistical nature, the RETIRA index is intrinsically exposed to signal outliers due to occasional natural (Aliano et al., 2008a) or observational (see Filizzola et al., 2004; Aliano et al., 2008b) phenomena. But this happens just in case they are actually rare for the considered location/time. Differently (i.e. if they are well statistically represented in the time-series) their occurrence will simply increase the normal signal variability (the numerator in Eqs. (1) and (2)) consequently reducing the possibility for the ALICE and RETIRA indices to reach high values. From this point of view RST approach is intrinsically protected from the possibility of false anomalies proliferation. In the others (rare) cases, the specific spatio-temporal characteristics of these signal variations (small duration, often known date of occurrence and typical spatial distribution, e.g. Filizzola et al., 2004; Tramutoli et al., 2005; Eleftheriou et al., 2016) help to define, isolate and discard such outliers (e.g. requiring spatio-temporal persistence, Tramutoli et al. 2005) from further analyses. Nevertheless, it has been shown that a cloudy fraction of land portion of the scene more than 80%, can determine the values of $V(t)$ making the considered signal $\Delta V(r,t)$ not representative of the actual conditions of cloud-free pixels (Eleftheriou et al., 2016). For this reason, all images with cloud fraction more than 80% were excluded from the reference fields computation.

4. Methods

The RST approach considers each anomaly in the space–time domain as a deviation from a normal state that can be defined by processing multi-year time series of homogeneous (e.g. same month, same spectral channel/s; same overpass times) cloud-free satellite records.

The ALICE (Absolutely Llocal Index of Change of Environment) index gives a measure of such deviation being defined as follows:

$$\otimes_V(r,t') = \frac{V(r,t') - \mu_V(r)}{\sigma_V(r)} \quad (1)$$

where:

$r = (x,y)$ represents the coordinates of each pixel on the satellite image and t' is the time of acquisition of the satellite image, with $t' \in \tau$, where τ defines the homogenous domain of satellite imagery collected in the same time (hour) of the day and the same month of the year.

$V(r,t')$ is the spatial/temporal variable measured at site r, at the time t', $\mu_V(r)$ refers to time average and $\sigma_V(r)$ to the standard deviation of $V(r,t')$ at site r, computed on cloud-free data from satellite images belonging to selected homogenous datasets ($t' \in \tau$).

The variable V as well as the used reference field $\mu_V(r)$ are subject to different choices depending on the applications (Tramutoli, 1998, Tramutoli, 2007). A specific ALICE index was introduced to identify subtle variations of the Earth's thermally emitted radiation further reducing "natural noise" due to the possible seasonal/climatological fluctuations of the temperature field at a large scale. It was named RETIRA (Robust Estimator of TIR Anomalies; Tramutoli et al., 2001; Filizzola et al., 2004, Tramutoli et al., 2005) and defined as:

$$\otimes_{\Delta T}(r,t') = \frac{\Delta T(r,t') - \mu_{\Delta T}(r)}{\sigma_{\Delta T}(r)} \quad (2)$$

where the generic variable $V(r,t')$ in the definition (1) of the ALICE index was substituted by the specific variable:

$\Delta T(r,t') = T(r,t') - T(t')$ which represents the difference between the current Thermal InfraRed (TIR) signal value $T(x,y,t)$ measured at site r, and its spatial average $T(t)$, computed in place on the image, taking into account only cloud-free pixels, all belonging to the same, land or sea -according to where the r is located over the area-, class in the study area.

The RETIRA index provides an estimation of the local (spatial–temporal) excess of the current $\Delta T(r, t')$ signal compared with its historical mean value $\mu_{\Delta T}(r)$, weighted by its variability $\sigma_{\Delta T}(r)$ at the considered location. The latter includes all the possible noise sources, which are not related to the event to be monitored. The use of $\Delta T(r,t)$

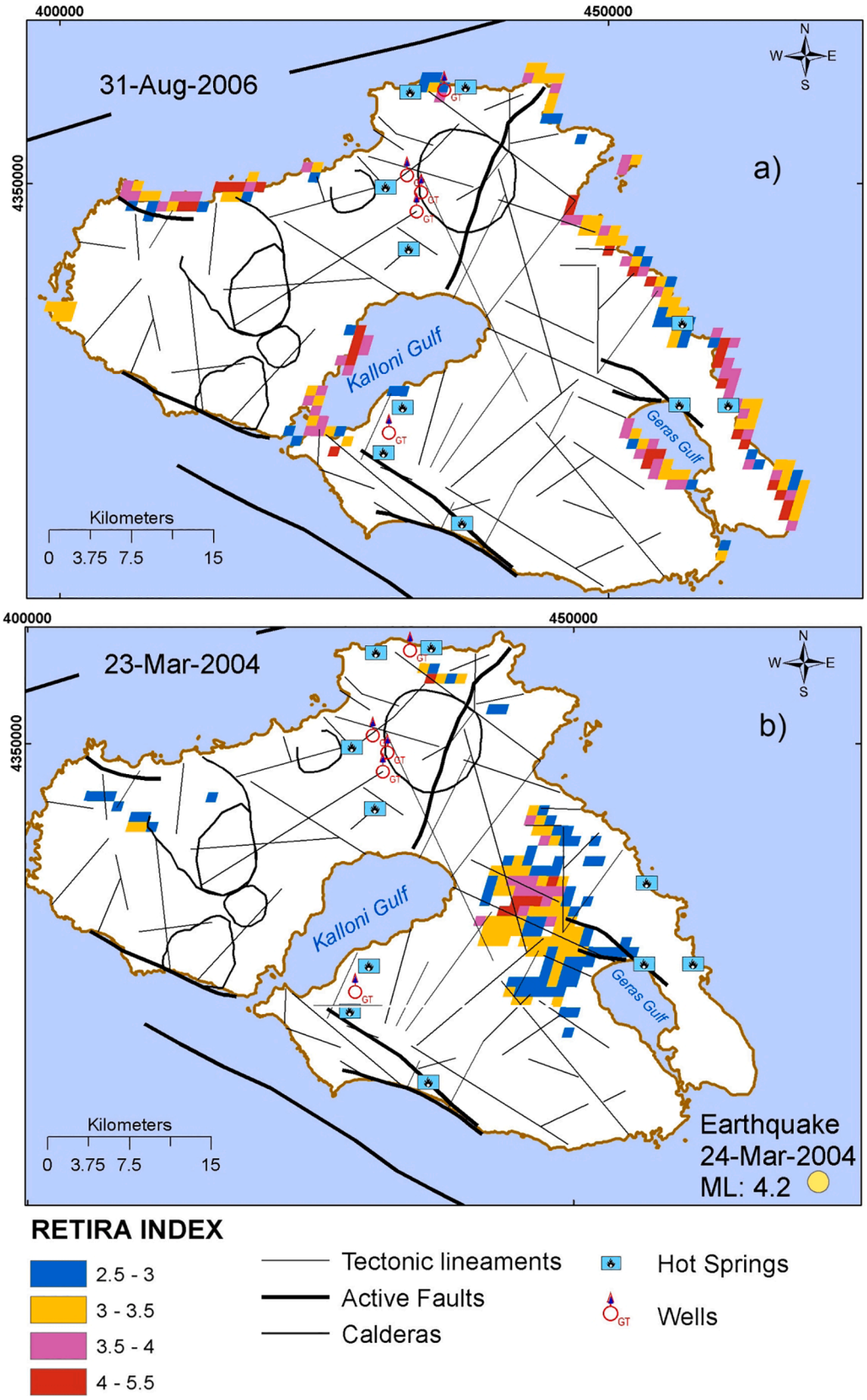

Fig. 3. Two examples of RETIRA thermal anomalies excluded from further analyses: (a) Spurious thermal anomalies (artifacts) along the coastlines due to well known (Filizzola et al., 2004; Aliano et al., 2008b; Genzano et al., 2015) effects due to navigation/co-location errors in the processing of MODIS LST product image. (b) RETIRA thermal anomalies map excluded by further analyses because possibly (following Eleftheriou et al., 2016) associated with an earthquake (4.2 M_L) occurred the day after (epicenter indicated by a yellow circle). (For interpretation of the references to color in this figure legend, the reader is referred to the web version of this article.)

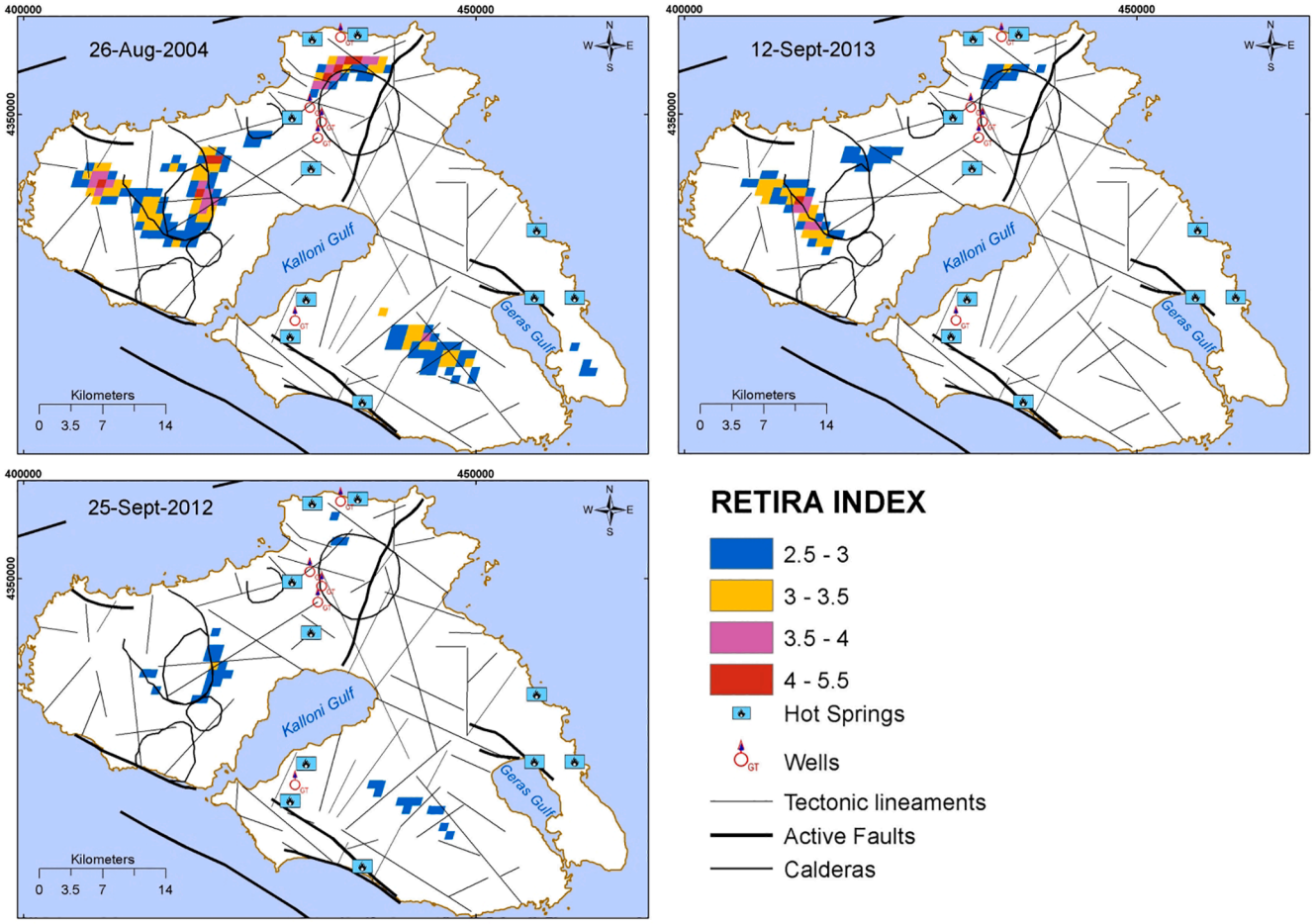

Fig. 4. Maps of residual RETIRA thermal anomalies combined with the major faults and caldera structures of the Lesvos Island. Colorized pixels represent thermal anomalies (over 2.5) corresponding to different RETIRA values. In these examples, the thermal anomalies appear to occur mainly along the caldera rims and ring faults associated with the evolution of the Sigri (to the northwest) and Stipsi (to the northeast) calderas.

instead of $T(r,t)$ reduces the possible contributions due to day-to-day and/or year-to-year climatological changes (e.g., occasional warming) and/or season time-drifts. Both e $\mu_{\Delta T}(r)$ and $\sigma_{\Delta T}(r)$ are computed for each location r, by processing several years of satellite records acquired under similar observational conditions. The signal - i.e. the numerator in the expression (2) - is evaluated by comparison with the corresponding natural/observational noise (N) (i.e., the standard deviation, $\sigma_{\Delta T}(r)$). In this way, the intensity of anomalous TIR transients can be evaluated in terms of the signal-to-noise ratio. Tramutoli et al. (2001) showed that the RETIRA index emphasizes low-level thermal anomalies regardless of sources of natural/observational noise. Like all ALICE indices, also RETIRA is (in principle) a Gaussian standardized variable (with expected values $\mu \sim 0$ and $\sigma \sim 1$), so that RETIRA values (in modulus) higher than 2 (3) have a probability of occurrence of 2,3% (0,13%). In this way the choice of its relative threshold value quantitatively qualifies how much rare (and significant) are the identified anomalies. In this study, we investigated the use of the RETIRA index applied to MODIS-LST data as a possible indicator of temporal variations in geothermal activity.

Moreover, a Sentinel-2A MSI L1C satellite dataset was processed - by using SNAP - (Sentinel Application Platform, European Space Agency, software, version 2.0.2) - for the mapping of hydrothermal alteration in the volcanic field of Lesvos. Firstly, the images were spatially subset to the study area extent, and then, Sentinel-2A MSI bands 4 (Red) and 8a (NIR) were used for the calculation of Normalized Difference Vegetation Index (NDVI). A conservative cutoff with NDVI > 0.4 was applied aiming to exclude densely vegetated areas from further analyses. As it is well known, due to the intrinsic thermoregulation capabilities of vegetation, geothermal alterations could be particularly difficult to identify, if not completely hidden. Afterwards, three band ratios originally proposed for Landsat 5 TM (Sabins, 1999), were selected for mapping the alteration mineralogy in the volcanic field of Lesvos. For this purpose, we used the bands 2 (Blue), 4 (Red), 11 (SWIR) and 12 (SWIR) of Sentinel-2A MSI. A combination that highlights hydroxyl bearing (Al-OH) alterations (Sentinel-2A MSI 11/12), a combination that highlights iron oxides (e.g. hematite and magnetite) in general (Sentinel-2A MSI 4/2) and a combination that highlights ferrous iron oxides (any mineral having a considerable portion of Fe^{2+} in its composition) (Sentinel-2A MSI 4/11) were finally chosen. The three band ratios were used to create a false color composite product.

5. Results and discussion

5.1. Identification of geothermal anomalies

In this section, we present results achieved using the RETIRA index to search for possible geothermal temporal anomalies in the area of Fig. 1. We considered as anomalous pixels those having values of the aforementioned index higher than 2.5 (0,6% of probability). As mentioned in the previous section, RETIRA anomalies can be expected not just in relation to variations in geothermal activity, but also as a consequence of other (rare) conditions related to natural events or to inadequate image processing. Moreover, a large literature (e.g. Tramutoli et al. 2015 and reference herein) reports of their appearance also in relation to some

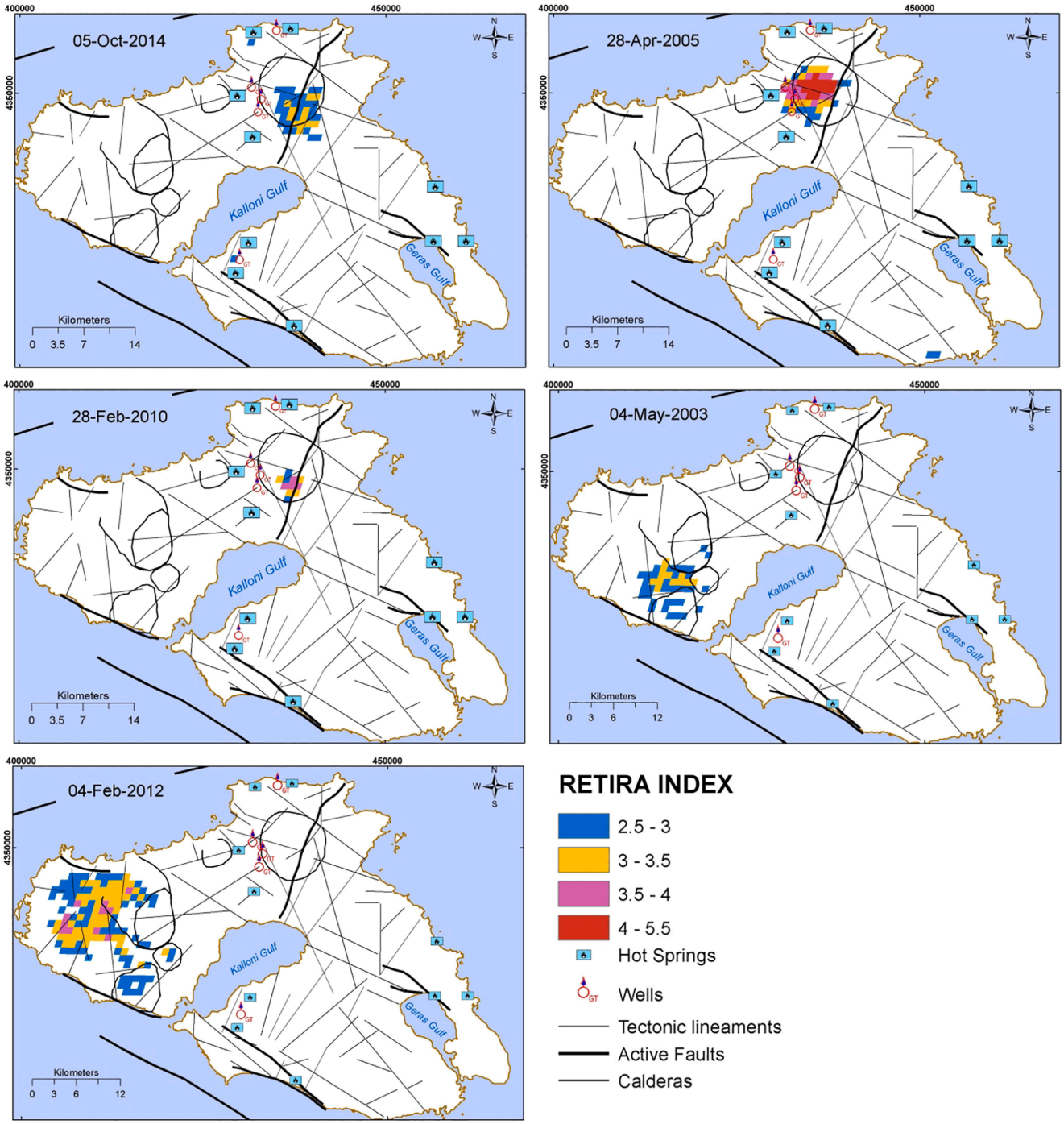

Fig. 5. Maps of residual RETIRA thermal anomalies combined with the major faults and caldera structures of the Lesvos Island. In these examples, the thermal anomalies appear to occur mainly in areas of known hydrothermal alterations inside Stipsi caldera (to the northeast) Sigri caldera (to the northwest) and Mesotopos caldera (to the southwest). Note the characteristic circular pattern of thermal anomalies in the Mesotopos caldera which is in a good spatial agreement with the previously reported circularly placed hydrothermally altered lava domes (see Kouli and St. Seymour, 2006 and Fig. 8b). Finally, the Sigri Petrified Forest (see Fig. 1) seems to host extended thermal anomaly probably associated with the presence of dense faulting and hydrothermal alteration (Pe-Piper et al., 2019).

earthquake occurrence. A specific study performed over Greece by Eleftheriou et al. (2016) suggests, on the base of 10 years of continuous satellite observations (processed by a similar approach), that RETIRA anomalies appear (with only a 7% of false positives) in a non-casual relation with earthquakes of magnitude 4 or more occurring in a pre-defined temporal and spatial window. Therefore, we performed a preliminary assessment of achieved results in order to identify and discard those thermal anomalies for which, other possible causes (different from geothermal activity variations) can be invoked.

The daily analysis revealed that on 1654 imagery over 4353 analyzed (i.e. 38%) pixels with values of RETIRA index higher than 2.5 were present. As can be seen from Figs. 3–6, detected thermal anomalies contained also pixels with values of RETIRA index up to 5 (see red pixels). It is worth mentioning that out of 1654 images, 151 (i.e. about 9%) included false thermal anomalies associated with clouds or with inaccurate image navigation/co-location (see Fig. 3a). To exclude TIR anomalies possibly associated to seismic activity information provided by the "Institute of Geodynamics, National Observatory of Athens"

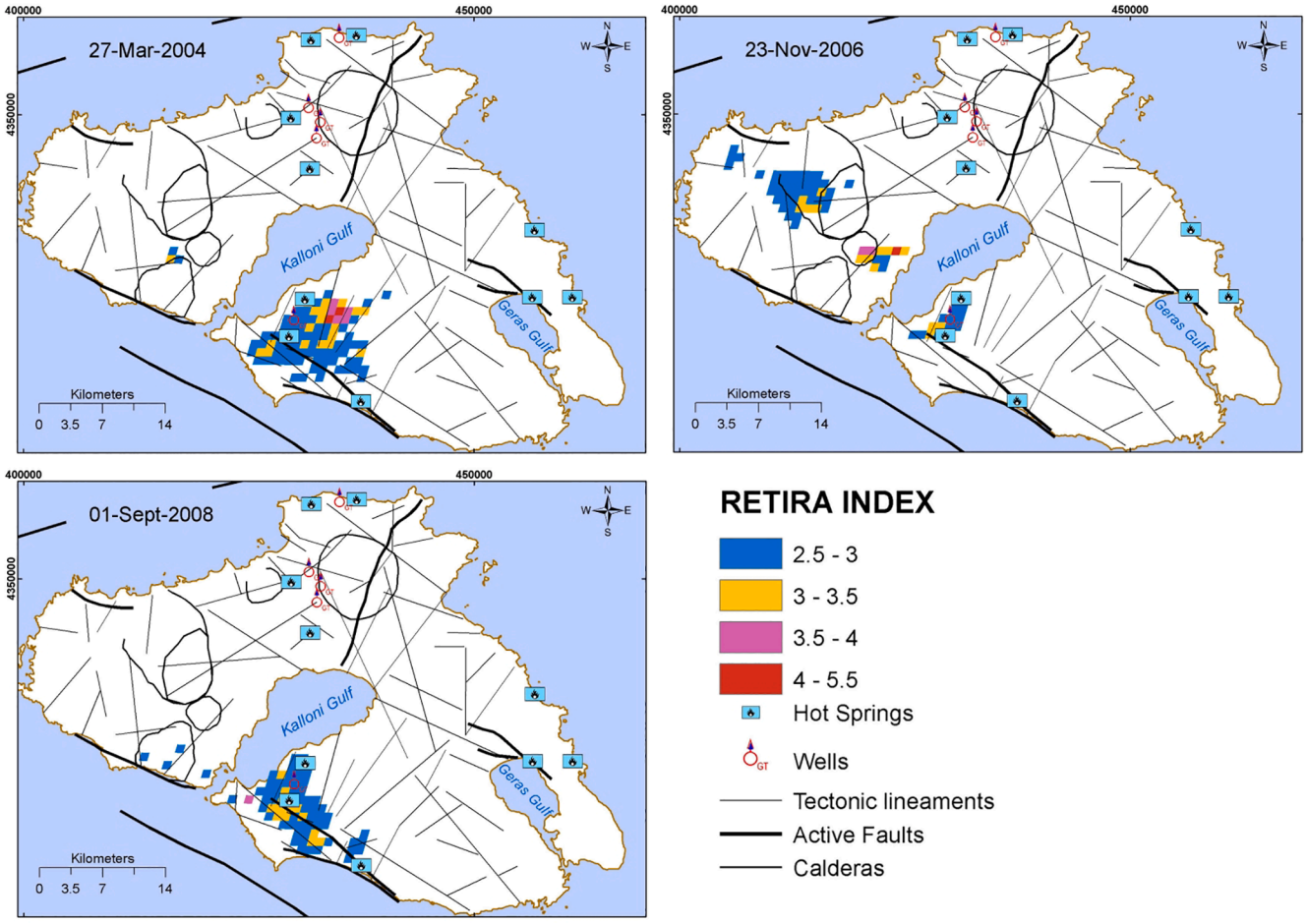

Fig. 6. RETIRA thermal anomaly maps of the geothermal field combined with the major faults and caldera structures of the Lesvos Island. In this case, thermal anomalies are spatially located on either side of the of the Polichnitos and Vatera fault system which according to Günther et al. (1977) controls the Polichnitos geothermal field and the local thermal springs. Some other thermally anomalous pixels spatially coincide with known hydrothermal alterations inside Mesotopos and Sigri calderas to the southwest and northwest, respectively.

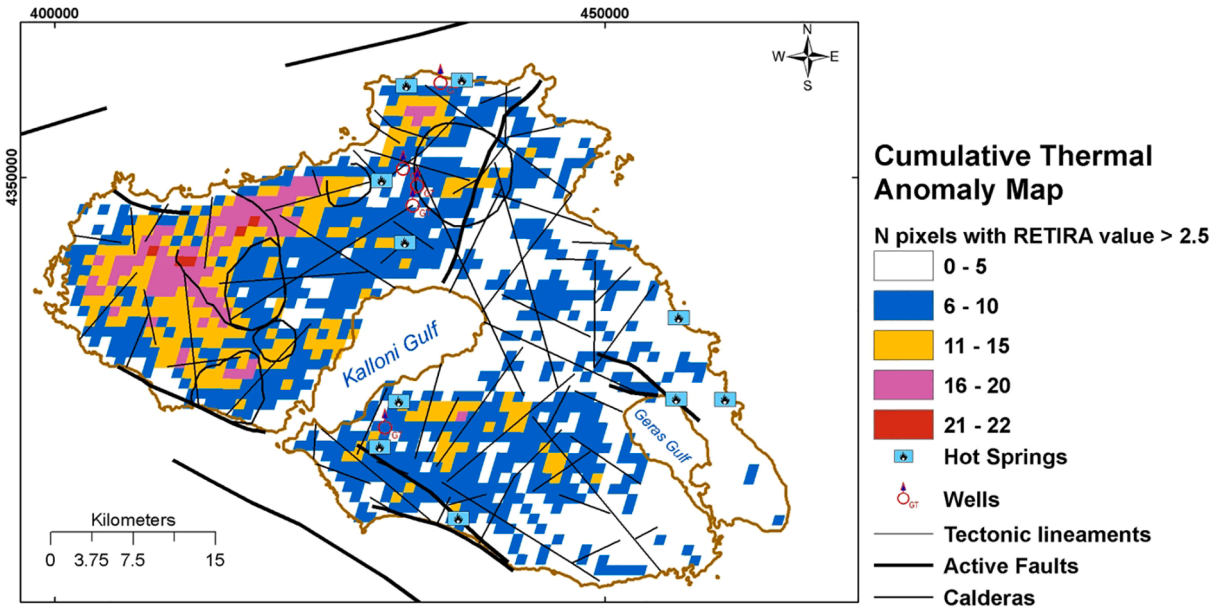

Fig. 7. Cumulative map counting for each pixel the number of times over-threshold values (i.e. RETIRA index greater than 2.5) are reached. Preferential spatial distribution of anomalies over time seems to concentrate to the Petrified Forest Area, to the northeastern part of Stipsi caldera where hot springs are located, inside Mesotopos caldera and to the broader Polichnitos area to the south of Lesvos Island.

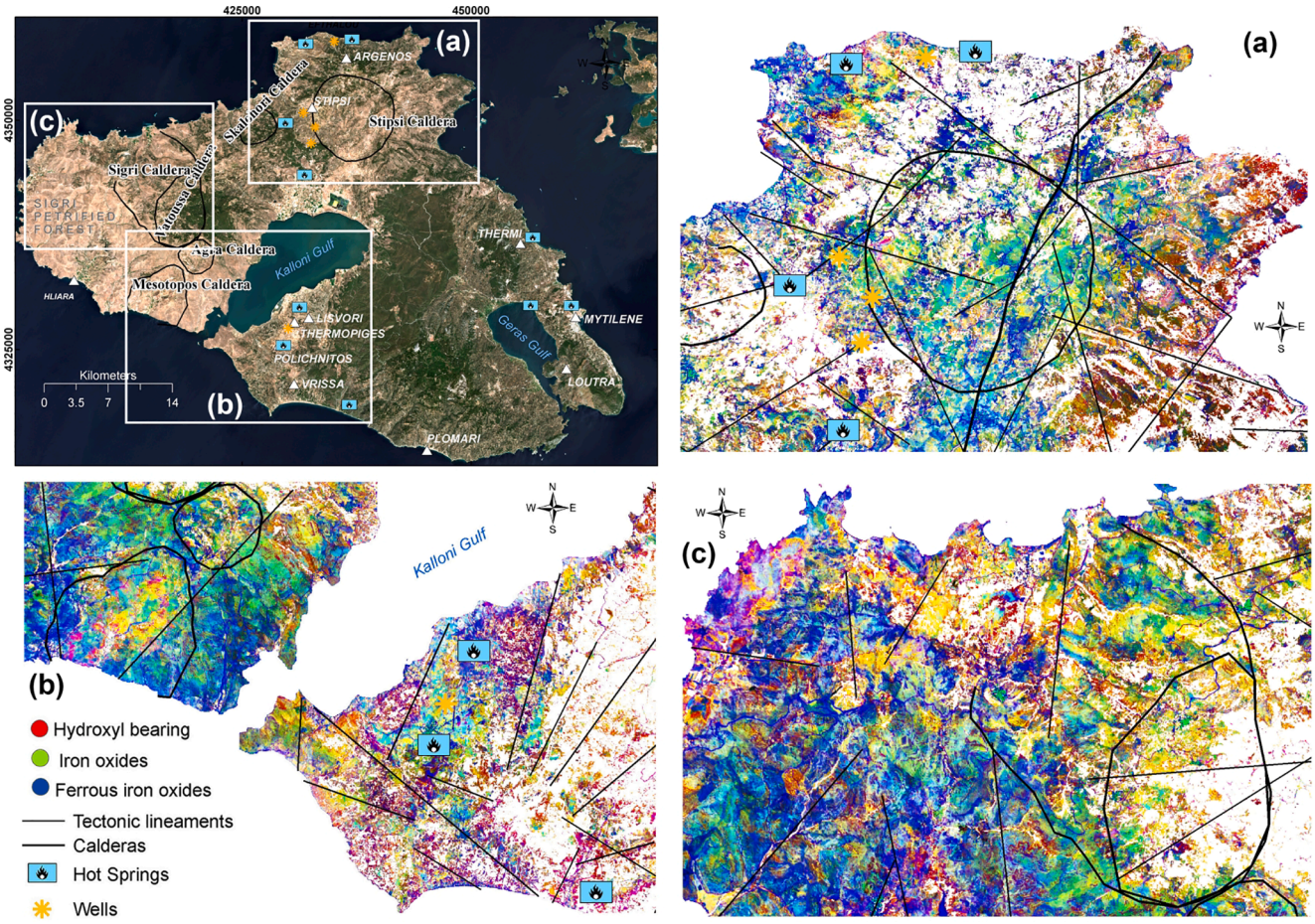

Fig. 8. Natural color composite of a Sentinel-2A MSI satellite image showing Lesvos island on 01/08/2017 and the produced false color composite (R,G,B) Sentinel-2A MSI 11/12, Sentinel-2A MSI 4/2, Sentinel-2A MSI 4/11 for; (a) Stipsi caldera (northeastern Lesvos), (b) Mesotopos and Agra calderas (southwestern Lesvos) and the opposite Polichnitos area and (c) Sigri caldera and Sigri Petrified Forest. In this product, the pixels with a relatively high value hydroxyl bearing alteration are shown in red. The iron oxides and the ferrous iron oxides are depicted in green and blue respectively. Areas with coexistence of hydroxyl bearing and iron oxide alterations are depicted with yellow colors while bluish-green areas exhibit both iron oxides and ferrous iron oxides. The circular yellow and pink structures inside Mesotopos calderas suggest the position of hydrothermally altered lava domes (see Fig. 5). (For interpretation of the references to color in this figure legend, the reader is referred to the web version of this article.)

(www.noa.gr) were also used. Following Eleftheriou et al. (2016) every satellite image with a detected anomaly was buffered with a zone of 150 km radius, searching for the occurrence of earthquakes with magnitude greater than 3.8 ML in a time-period of 15 days before and 30 days after the identification of the thermal anomaly. By comparing flagged thermal anomalies with NOA data, 680 of them falling in the previous space–time constrains, were excluded by the following analyses. Fig. 3b shows an example of such thermal anomalies (occurred on 23 March 2004) excluded for the effect of the previous selection rules in relation to the seismic event ($4.2M_L$) that occurred in the area on 24 March. Finally, we compared our dataset of thermal anomalies with those of NASA FIRMS Fire Archive (https://earthdata.nasa.gov/firms). This analysis revealed that 53 thermal anomalies were associated to fire events and then excluded from further analysis. After excluding all those features, the final dataset contained 770 thermal anomalies (representative examples are given in Figs. 4–6) for which, in our knowledge, no other possible origin (except intrinsic statistical fluctuations) can be hypothesized. A cumulative map counting for each pixel the number of times over-threshold values are reached was finally produced showing the preferential spatial distribution of anomalies over time (Fig. 7).

The possible association of these thermal anomalies with anomalous changes in geothermal activity was then investigated.

5.2. Integrating RETIRA index results with geological data

In order to test the hypothesis that residual thermal anomalies can be related to geothermal activity their possible spatial relation with geological characteristics of the Lesvos Volcanic field was investigated at first. Thermal anomalies along with several geological elements, such as calderas, caldera borders, tectonic faults, geothermal springs and hydrothermal alterations mapped by processing SENTINEL-2 MSI satellite images were introduced in a Geographic Information System (GIS) (Figs. 4–8).

As a result, the 770 thermal anomaly maps can be grouped into three general categories; (a) those showing anomalies mainly along Sigri (to the northwest) and Stipsi (to the northeast) caldera rims and ring faults associated with the evolution of these major calderas (Fig. 4), (b) those where thermal anomalies coincide with areas of known hydrothermal alterations either inside Stipsi caldera or Sigri and Mesotopos calderas (Figs. 5 and 8). In the case of Stipsi and Mesotopos caldera, thermal anomalies show a characteristic circular pattern which spatially agrees with the circular hydrothermal alterations revealed in Sentinel FCC (Fig. 8a and 8b). According to Kouli and St.Seymour (2006) these are post caldera hydrothermally altered lava domes placed across ring faults. Moreover, Sigri Petrified Forest (see Fig. 1) seems to host extended thermal anomalies probably associated with the presence of dense faulting and extended hydrothermal alteration (Fig. 8c) (Pe-Piper

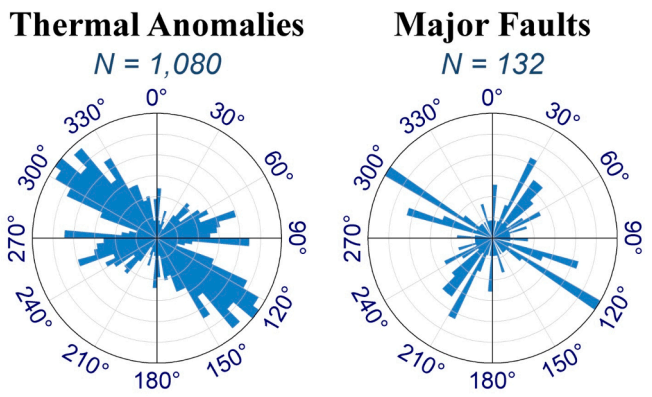

Fig. 9. The main orientation of both thermal anomalies and faults is the NW-SE.

et al., 2019) and (c) those with thermal anomalies spatially concentrated on either side of the Polichnitos and Vatera fault system which according to Günther et al. (1977) controls the Polichnitos geothermal field and the local thermal springs. The cumulative map of Fig. 7 shows the frequency of occurrences of the thermal anomaly during the 12 years of data analysis for each pixel. Preferential spatial distribution of anomalies over time seems to be concentrated in the Petrified Forest Area, in the northeastern part of Stipsi caldera where hot springs are located, inside Mesotopos caldera and in the broader Polichnitos area to the south of Lesvos Island.

The visual inspection of each one of the 770 thermal anomaly maps as well as of the cumulative map (Fig. 7), gives some indications for the spatial control of big tectonic lineaments over thermal anomalies. In many cases thermally anomalous pixels are located in the junction of two faults. In other cases an extended thermal anomaly is bordered by the existence of a fault, as in the cases of Stipsi caldera (Fig. 5) and Polichnitos (Fig. 6).

These visual observations are further confirmed by coincident major

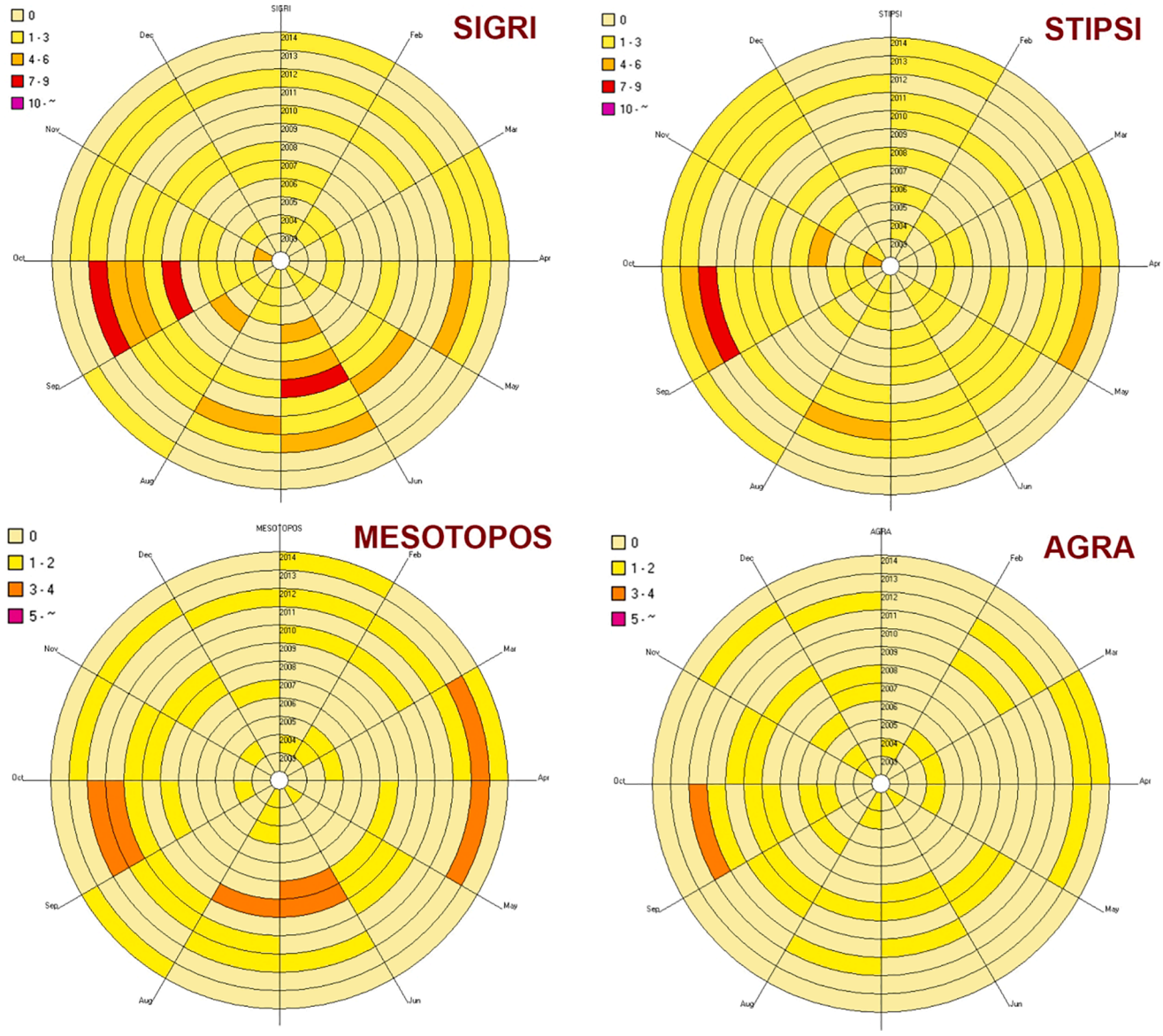

Fig. 10. Data clocks displaying the temporal distribution of thermal anomalies related to four of the major calderas of the Lesvos geothermal field. The Sigri volcanic structure hosts the majority of the mapped geothermal anomalies. Many of the geothermal anomalies mapped in Mesotopos caldera are also mapped in Agra since the two structures are proximal each other. Nevertheless, the geothermal activity of Mesotopos caldera seems to be more intense and this is in agreement with the extensively hydrothermally altered lava domes that are situated along the ring faults.

orientations (NW-SE and NE-SW) that exhibit both the rose diagrams created from thermal anomalies and Lesvos tectonic lineaments (Fig. 9).

Finally, data clocks (Fig. 10) display the temporal distribution of thermal anomalies related to four of the major calderas of the Lesvos geothermal field. The Sigri volcanic structure hosts the majority of the mapped geothermal anomalies probably because it represents the most extended and complex volcanic edifice (nested caldera) which is geologically connected with the extended hydrothermally altered Petrified Forest. The Stipsi caldera shows also frequent thermal anomalies as one of the two major calderas and as an area of well known hydrothermal alterations and epithermal mineralization. Many of the geothermal anomalies mapped in Mesotopos caldera were also mapped in Agra since the two structures are proximal to each other. Nevertheless, the geothermal activity of Mesotopos seems to be much more intense. This is in agreement with the extensively hydrothermally altered lava domes that are situated along the well-defined ring faults acting as fluid flow paths.

6. Conclusions

In this paper, we used MODIS (LST) data over a period of 12 years (2003–2014) to investigate the possible existence of anomalous changes in the active geothermal field of Lesvos Island. Therefore, our aim was not the detection of a geothermal field (it is quite well known from ground measurement of heat fluxes and extensive bibliographic references) but to investigate the possibility to monitor activity variations using thermal signatures and applying the RST techniques.

Thermal anomalies detected in the Miocene volcanic field of Lesvos Island usually coincide with caldera rims and hydrothermally altered rocks (Stipsi, Sigri and Mesotopos calderas) while in other cases they are spatially correlated with major tectonic faults and known geothermal springs as in the case of Polichnitos. Taking into consideration the approximately 20 ma age of Lesvos volcanic terrain, we suggest that the geodynamic environment of the broader area keeps alive the geothermal field and it is maybe associated with the recorded geothermal variations. A probable explanation of the temporal variation in the geothermal activity could be the uplifting and circulation of the hydrothermal waters through radial and tectonic faults due to changes of the sub-surface physicochemical processes. For instance, micro-fracturing can lead to permeability changes and episodic gas injection into the hydrothermal system. In the Lesvos densely faulted and heavily eroded volcanic terrain, a probable episode of increase in fluid infusion due to tectonic activity in the multi-fractured lithosphere, could be superficially expressed in areas of high permeability structures which act as pathways to fluid circulation. Such areas are usually pre-existing faults, fault intersections and volcanic structures.

In conclusion, the monitoring of geothermal anomalies from time-series satellite imagery and geological field data (e.g. geologic maps) could provide promising indications to the scientific community for future work. In this direction, the RST techniques, and in particular the use of the RETIRA index, may represent a valuable tool in geothermal field analysis, since mapped thermal anomalies can act as a guide for localization of mineral alterations and hydrothermal routes mapping.

Declaration of Competing Interest

The authors declare that they have no known competing financial interests or personal relationships that could have appeared to influence the work reported in this paper.

Acknowledgments

The authors thank Dr Karen St.Seymour for constructively and carefully reviewing this paper.

References

Andritsos, N., Arvanitis, A., Papachristou, M., Fytikas, M. Dalambakis, P., 2010. Geothermal activities in Greece during 2005-2009. Proceedings World Geothermal Congress, Bali, Indonesia.

Aguilar-Lome, J., Espinoza-Villar, R., Espinoza, J.C., Rojas-Acuña, J., Willems, B.L., Leyva-Molina, W.M., 2019. Elevation-dependent warming of land surface temperatures in the Andes assessed using MODIS LST time series (2000–2017). Int. J. Appl. Earth Obs. 77, 119–128.

Aliano, C., Corrado, R., Filizzola, C., Genzano, N., Pergola, N., Tramutoli, V., 2008a. Robust TIR satellite techniques for monitoring earthquake active regions: limits, main achievements and perspectives. Ann. Geophys. 51, 303–317.

Aliano, C., Corrado, R., Filizzola, C., Pergola, N., Tramutoli, V., 2008b. Robust satellite techniques (RST) for the thermal monitoring of earthquake prone areas: the case of Umbria-Marche October, 1997 seismic events. Ann. Geophys. 51, 451–459.

Anderson, M., Kustas, W., 2008. Thermal remote sensing of drought and evapotranspiration. EOS T. Am. Geophys. Un. 89, 233–234.

Anderson, M.C., Allen, R.G., Morse, A., Kustas, W.P., 2012. Use of Landsat thermal imagery in monitoringevapotranspiration and managing water resources. Remote Sens. Environ. 122, 50–65.

Brunsell, N.A., Gillies, R.R., 2003. Determination of scaling characteristics of AVHRR data with wavelets: Application to SGP97. Int. J. Remote Sens. 24, 2945–2957.

Cannatelli, C., Spera, F.J., Bodnar, R.J., Lima, A., De Vivo, B., 2020. Ground movement (bradyseism) in the Campi Flegrei volcanic area: a review. Vesuvius, Campi Flegrei, and Campanian Volcanism, Elsevier 407–433.

Chatzipetros, A., Kiratzi, A., Sboras, S., Zouros, N., Pavlides, S., 2013. Active faulting in the north-eastern Aegean Sea Islands. Tectonophysics 597–598, 106–122.

Christman, Z., Rogan, J., Eastman, J.R., Turner, B.L., 2016. Distinguishing land change from natural variability and uncertainty in central Mexico with MODIS EVI, TRMM precipitation, and MODIS LST data. Remote Sens. 8, 478.

Eleftheriou, A., Filizzola, C., Genzano, N., Lacava, T., Lisi, M., Paciello, R., Pergola, N., Vallianatos, F., Tramutoli, V., 2016. Long-term RST analysis of anomalous TIR sequences in relation with earthquakes occurred in Greece in the period 2004–2013. Pure Appl. Geophys. 173, 285–303.

Eleftheriou, D., Kiachidis, K., Kalmintzis, G., Kalea, A., Bantasis, C., Koumadoraki, P., Spathara, M.E., Tsolaki, A., Tzampazidou, M.I., Gemitzi, A., 2018. Determination of annual and seasonal daytime and nighttime trends of MODIS LST over Greece-climate change implications. Sci. Total Environ. 616, 937–947.

Faulds, J.E., Coolbaugh, M.F., Vice, G.S., Edwards, M.L., 2006. Characterizing structural controls on geothermal fields in the northwestern Great Basin: a progress report. GRC Trans. 30, 69–76.

Faulds, J.E., Henry, C.D., 2008. Tectonic influences on the spatial and temporal evolution of the Walker Lane: An incipient transform fault along the evolving Pacific – North American plate boundary. In: Spencer, J.E., Titley, S.R. (Eds.), Circum-Pacific Tectonics, Geologic Evolution, and Ore Deposits: Tucson. Arizona Geological Society, Digest, pp. 437–470.

Faulds, J.E., Hinz, N., Kreemer, C., Coolbaugh, M., 2012. Regional patterns of geothermal activity in the great basin region, Western USA: correlation with strain rates. GRC Trans 36, 897–902.

Filizzola, C., Pergola, N., Pietrapertosa, C., Tramutoli, V., 2004. Robust satellite techniques for seismically active areas monitoring: a sensitivity analysis on September 7, 1999 Athens's earthquake. Phys. Chem. Earth, PT A/B/C 29, 517–527.

Fred, G.R., Watson, R.E., Lockwood, W.B., Newman, T.N., Anderson, R.A.G., 2008. Development and comparison of Landsat radiometric and snowpack model inversion techniques for estimating geothermal heat flux. Remote Sens. Environ. 112, 471–481.

Fytikas, M., Andritsos, N., Dalabakis, P., Kolios, N., 2005. Greek geothermal update 2000–2004. Proc. World Geothermal Congress April, 24–29.

Ganas, A., Oikonomou, I., Tsimi, C., 2013. NOAfaults: a digital database for active faults in Greece. Bull. Geol. Soc. Greece 47 (2), 518–530.

Genzano, N., Filizzola, C., Paciello, R., Pergola, N., Tramutoli, V., 2015. Robust Satellite Techniques (RST) for monitoring earthquake prone areas by satellite TIR observations: the case of 1999 Chi-Chi earthquake (Taiwan). J. Asian Earth Sci. 114, 289–298.

Guido, D.M., Campbell, K.A., 2011. Jurassic hot spring deposits of the Deseado Massif (Patagonia, Argentina): characteristics and controls on regional distribution. J. Volcanol. Geoth. Res. 203, 35–47.

Günther, R., Kappelmeyer, O., Kronberg, P., 1977. Zur prospektion auf geothermale anomalien, erfahrungen einer modelluntersuchung in Polichnitos, Lesbos (Griechenland). Geol. Rundsch. 66, 10–33.

Hacıoğlu, O., Başokur, A.T., Diner, H., Meqbel, N., Arslan, H.İ., Oğuz, K., 2020. The effect of active extensional tectonics on the structural controls and heat transport mechanism in the Menderes Massif geothermal province: Inferred from three-dimensional electrical resistivity structure of the Kurşunlu geothermal field (Gediz Graben, western Anatolia). Geothermics 85, 101708.

Jackson, J., McKenzie, D., 1988. The relationship between plate motions and seismic moment tensors, and the rates of active deformation in the Mediterranean and Middle East. Geophys. J. Int. 93 (1), 45–73.

Le Pichon, X., Chamot-Rooke, N., Lallemant, S., Noomen, R., Veis, G., 1995. Geodetic determination of the kinematics of central Greece with respect to Europe: implications for eastern Mediterranean tectonics. J. Geophys. Res. 100, 12675–12690.

Le Pichon, X., Kreemer, C., 2010. The Miocene-to-Present kinematic evolution of the eastern Mediterranean and Middle East and its implications for dynamics. Annu. Rev. Earth Planet. Sci. 38, 323–351.

Karnieli, A., Agam, N., Pinker, R.T., Anderson, M., Imhoff, M.L., Gutman, G.G., Panof, N., Goldberg, A., 2010. Use of NDVI and land surface temperature for drought assessment: Merits and limitations. J. Climate 23, 618–633.
Kelepertsis, A.E., Esson, J., 1987. Major and trace element mobility in altered volcanic rocks near Stypsi, Lesvos, Greece and genesis of a Kaolin deposit. Appl. Clay Sci. 2, 11–28.
Kelepertsis, A.E., 1993. Hydrothermal alteration of basic island-arc volcanic rocks north and south of Mytilini Town, Lesvos Island, Greece. Terra Nova 5, 52–60.
Keramitsoglou, I., Chris, T., Kiranoudis, C.T., Ceriola, G., Weng, Q., Rajasekar, U., 2011. Identification and analysis of urban surface temperature patterns in Greater Athens, Greece, using MODIS imagery. Remote Sens. Environ. 115, 3080–3090.
Kouli, M., Seymour, K.S.St., 2006. Contribution of remote sensing techniques to the identification and characterization of Miocene calderas, Lesvos Island, Aegean Sea, Hellas. Geomorphology 77, 1–16.
Krupp, R.E., Seward, T.M., 1987. The Rotokawa geothermal system, New Zealand. Econ. Geol. 82, 1109–1129.
Kustas, W., Anderson, M., 2009. Advances in thermal infrared remote sensing for land surface modelling. Agr. Forest Meteorol. 149, 2071–2081.
Lambrakis, N., Katsanou, K., Siavalas, G., 2014. Geothermal fields and thermal waters in Greece: An overview. Geotherm. Syst. Energy Resour.: Turkey and Greece Chapter 3, 25–45.
Lee, K., 1978. Analysis of thermal infrared imagery of the Black Rock Desert geothermal area. Colorado School of Mines Quarterly 4, 31–44.
Li, T., Lv, G., Wen, Y., 2012. Application of land surface temperature inversion based on emissivity mixture analysis at sub-pixel scale in geothermal exploration. In Earth Observation and Remote Sensing Applications (EORSA). Second International Workshop, pp. 139–143.
Li, Z.L., Tang, B.H., Wu, H., Ren, H., Yan, G., Wan, Z., Sobrino, J.A., 2013. Satellite-derived land surface temperature: Current status and perspectives. Remote Sens. Environ. 131, 14–37.
Littlefield, E.F., Calvin, W.M., 2014. Geothermal exploration using imaging spectrometer data over Fish Lake Valley, Nevada. Remote Sens. Environ. 140, 509–518.
Lillesand, T.M., Kiefer, R.W., Chipman, J.W., 1987. Remote Sensing and Image Interpretation. John Wiley & Sons, New York.
McKenzie, D., 1972. Active tectonics of the Mediterranean region. Geoph. J. R. Astron. Soc. 30, 109–182.
Mendrinos, D., Choropanitis, I., Polyzou, O., Karytsas, C., 2010. Exploring for geothermal resources in Greece. Geothermics 39, 124–137.
Mercier, J.L., Sorel, D., Vergely, P., Simeakis, K., 1989. Extensional tectonic regimes in the Aegean basins during the Cenozoic. Basin Res. 2, 49–71.
Miliaresis, G., 2012. Selective variance reduction of multi-temporal LST imagery in the East Africa Rift System. Earth Sci. Inform. 5, 1–12.
Moeck, I.S., 2014. Catalog of geothermal play types based on geologic controls. Renew. Sustain. Energy Rev. 37, 867–882.
Pe-Piper, G., 1980. The Cenozoic volcanic sequence of Lesbos, Greece. Z. Dtsch. Geol. Ges. 131, 889–901.
Pe-Piper, G., Piper, D.J.W., 1993. Revised stratigraphy of the Miocene volcanic rocks of Lesbos, Greece. Neues Jahrb Geol. P. 2, 97–110.
Pe-Piper, G., Imperial, A., Piper, D.J.W., Zouros, N.C., Anastasakis, G., 2019. Nature of the hydrothermal alteration of the Miocene Sigri Petrified Forest and host pyroclastic rocks, western Lesbos, Greece. J. Volcanol. Geotherm. Res. 369, 172–187.
Prakash, A., Saraf, A.K., Gupta, R.P., Dutta, M., Sundaram, R.M., 1995. Surface thermal anomalies associated with underground fires in Jharia coal mines, India. Int. J. Remote Sens. 16, 2105–2109.
Qin, Q., Zhang, N., Nan, P., Chai, L., 2011. Geothermal area detection using Landsat ETM + thermal infrared data and its mechanistic analysis - A case study in Tengchong, China. Int. J. Appl. Earth Obs. 13, 552–559.
Roussos, N., Lyssimachou, T., 1991. Structure of the Central North Aegean Trough: An active strike-slip deformation zone. Basin Res. 3, 37–46.
Rokos, D., Argialas, D., Mavrantza, R., Seymour, K.St., Vamvoukakis, C., Kouli, M., Lamera, S., Paraskevas, H., Karfakis, I., Denes, G., 2000. Structural analysis for gold mineralization using remote sensing and geochemical techniques in a GIS environment: Island of Lesvos, Hellas. Nat. Resour. Res. 9, 277–293.
Sabins, F.F., 1999. Remote sensing for mineral exploration. Ore Geol. Rev. 14, 157–183.
Scambos, T.A., Campbell, G.G., Pope, A., Haran, T., Muto, A., Lazzara, M., Reijmer, C.H., van den Broeke, M.R., 2018. Ultralow surface temperatures in East Antarctica from satellite thermal infrared mapping: The coldest places on Earth. Geophys. Res. Lett. 45, 6124–6133.
Sillitoe, R.H., 1993. Epithermal models: genetic types, geometrical controls and shallow features. In: Kirkham, R.V., et al. (Eds.), Mineral Deposit Modeling: Geological Association of Canada, Special Volume, 40, pp. 403–417.
Stroppiana, D., Antoninetti, M., Brivio, P.A., 2014. Seasonality of MODIS LST over Southern Italy and correlation with land cover, topography and solar radiation. Eur. J. Remote Sens. 47, 133–152.
Tramutoli, V., 1998. Robust AVHRR Techniques (RAT) for Environmental Monitoring: theory and applications. In: Zilioli, E., (ed) Proc. SPIE, pp. 101–113.
Tramutoli, V., 2007. Robust satellite techniques (RST) for natural and environmental hazards monitoring and mitigation: theory and applications. Int. Work. Anal. Multi-temporal Remote Sens. Images. IEEE 1–6.
Tramutoli, V., Cuomo, V., Filizzola, C., Pergola, N., Pietrapertosa, C., 2005. Assessing the potential of thermal infrared satellite surveys for monitoring seismically active areas: The case of Kocaeli (Izmit) earthquake, August 17, 1999. Remote Sens. Environ. 96, 409–426.
Tramutoli, V., Di Bello, G., Pergola, N., Piscitelli, S., 2001. Robust satellite techniques for remote sensing of seismically active areas. Ann di Geofis. 44, 295–312.
Vamvoukakis, C., Seymour, K.St., Kouli, M., Lamera, S., Denes, G., 2005. Investigation of non pristine volcanic structures acting as probable hosts to epithermal gold mineralization in the back arc region of the active Aegean arc, using combined satellite imagery and field data: examples from Lesvos volcanic terrain. Developments in Volcanology 7, 329–343.
Vollmer, M., Möllmann, K.P., 2017. Infrared thermal imaging: fundamentals, research and applications. John Wiley & Sons, 2nd Edition.
Wan, Z., 2006. MODIS Land Surface Temperature products user's guide, Santa Barbara, CA. http://www.icess.ucsb.edu/modis/LstUsrGuide_v5/MODIS_LST_products_Users_guide.pdf.
Zouzias, D., Miliaresis, G.C., Seymour, K.St., 2011. Probable regional geothermal field reconnaissance in the Aegean region from modern multi-temporal night LST imagery. Environ. Earth Sci. 62, 717–723.